IET Electric Power Applications

Research Article

IET Journals
The Institution of Engineering and Technology

Non-intrusive induction motor speed detection

ISSN 1751-8660
Received on 25th September 2014
Revised on 25th December 2014
Accepted on 5th January 2015
doi: 10.1049/iet-epa.2014.0274
www.ietdl.org

Uzoma A. Orji, Zachary Remscrim, Christopher Schantz, John Donnal, James Paris, Mark Gillman, Kawin Surakitbovorn, Steven B. Leeb ✉, James L. Kirtley

Laboratory for Electromagnetic and Electronic Systems, MIT, Cambridge, MA, USA
✉ *E-mail: sbleeb@mit.edu*

Abstract: This paper presents an algorithm that enables estimation of the speed of a single induction motor in an aggregate current signal supplying several motors from a common utility feed. This algorithm maintains accuracy of speed estimation while using shorter lengths of data, and can distinguish the activation of individual motors in the aggregate signal. The ability to separate and track distinct motor harmonics in an aggregate current signal opens the door to non-intrusive energy scorekeeping and diagnostics for systems like air conditioning that operate under closed-loop control. New experimental results demonstrate the approach for these air-conditioning components in real buildings.

1 Smart monitoring

Smart grid and smart meter initiatives hope to allow energy providers and consumers to intelligently manage their energy needs through real-time monitoring, analysis and control of electrical power usage. The U.S. Department of Energy has identified 'sensing and measurement' as one of the 'five fundamental technologies' essential for driving the creation of a 'Smart Grid' [1]. The methods described in this paper estimate non-intrusively sense speed for a single motor operating in a collection of motors, and could be used to provide detailed energy scorekeeping and diagnostic measurements for electric machines for new metering functions.

Subtle harmonics associated with the rotor of a motor are modulated, spaced periodically in multiples of the line frequency [2, 3]. These rotor frequency harmonics can be used to determine the operating speed of a motor and have been used as the basis for diagnostic algorithms for detecting motor pathologies [4–7]. This paper introduces an algorithm that enables estimation of motor slot harmonics in an aggregate current signal supplying several motors from a common utility feed. The speed and operating schedule of a motor can be determined non-intrusively from an aggregate current feed serving many motors. This algorithm maintains accuracy of speed estimation while using shorter lengths of data, and can distinguish the activation of individual motors in the aggregate signal. This paper demonstrates that special attention can be paid to the aggregate current frequency content just before and just after a turn-on transient using non-intrusive load monitoring. These 'pre-transient' and 'post-transient' windows can be used to identify key harmonics that are not line locked, but which are indicative of rotor speed and pathological conditions in the motor, advancing the speed estimator presented in [8]. The ability to separate and track distinct motor harmonics in an aggregate current signal opens the door to non-intrusive energy scorekeeping and diagnostic for systems that operate under closed-loop control, like heating, ventilation and air-conditioning (HVAC) systems.

For example, a number of surveys of airflow and compressor faults in buildings hint at the range and extent of these problems. One compendium of fault surveys [9], which examined 503 rooftop air-conditioning units in 181 buildings in five states in the Western U.S. from 2001–2004, found that the airflow was out of the specified range in ~42% of the units surveyed. A separate study [10] of 4168 commercial air-conditioners in California reported that 44% of the surveyed units had airflow that was out of specifications. Studies of 29 new homes in Washington State [11] found that average duct leakage rates to the exterior ranged from 687 to 140 cubic feet per minute. Extrapolating from such fault surveys, one estimate for the total energy consumed by duct leakage is $5 billion/year [12]. If the speed of critical motors can be tracked for an HVAC system, the operating and diagnostic condition of fans and compressors can be inferred from motor shaft speed estimates [8].

This paper focuses on induction machines to experimentally demonstrate the proposed signal processing technique. The technique could be used, however, with any motor or any load that consumes a detectable harmonic current that is not a multiple of the line frequency. Harmonic current content tends to be present in induction machines of all types, including both single- and three-phase machines [13]. Even motor design features like skewed rotor bars tend to leave some harmonic variation in the permeance of a machine as a function of rotation [13], and this variation leads to harmonic currents that can be tracked by the methods introduced here. The algorithm demonstrated in this paper builds on the harmonic estimation algorithm presented in [8]. Here, we demonstrate that a non-intrusive load monitor (NILM) with transient event recognition [14] can serve as a platform for identifying induction motor speed in an aggregate data stream. The approach is described analytically and demonstrated experimentally, providing the raw speed information needed to track both normal and also pathological operation while eliminating the need for a sensor for every motor.

2 Rotor slot harmonics

Rotor slot harmonics are widely used in speed estimation algorithms. Other harmonics appear in the stator current of a motor which often make the task of searching for these rotor slot harmonics more difficult. Motors can experience various kinds of mechanical failures or faults that inject their own set of harmonics into the stator current. The utility line supplying current to the stator may have its own distortions that present troublesome harmonics, especially in the non-intrusive monitoring environment where a monitored current powers a collection of loads.

Rotor slot harmonics present in the stator current of a motor arise from the interaction between the permeance of the machine and the magnetomotive force (MMF) of the current in the stator windings. As the motor turns, the rotor slots filled with relatively low

permeability metal alter the effective length of the airgap, thereby affecting the permeance of the machine. This behaviour is seen in the flux, which is the product of the MMF and the permeance across the airgap. The odd harmonics present in the stator voltage introduce additional current harmonics. Static and dynamic eccentricity harmonics also appear in the stator current as the rotor turns irregularly in relation to the stator.

The slot harmonics, including the principal slot harmonic (PSH), are located at frequencies

$$f_{\text{sh}} = f\left[(kR + n_d)\frac{1-s}{p} + \nu\right] \tag{1}$$

where f is the supply frequency; $k = 0, 1, 2...$; R is number of rotor slots; $n_d = 0, \pm 1, ...$ is the order of rotor eccentricity or decentring as it rotates with respect to the stator; s is the slip, p is the number of pole pairs and $\nu = \pm 1, \pm 3, ...$ is the stator MMF harmonic order [3, 15].

Previous research has studied the effects of mechanical faults on the stator current spectrum [4, 6, 7, 16–25]. These faults, including broken rotors bars, damaged and failed bearings, rotor eccentricity, rotor asymmetry and shaft speed oscillations, produce distinct harmonics in the current spectrum. One mechanical fault of interest is the shaft speed oscillation, which can be enhanced when an imperfectly balanced fan is attached to the motor shaft. The frequencies of interest [18] are predicted by

$$f_{\text{sso}} = f\left[k\left(\frac{1-s}{p}\right) \pm \nu\right] \tag{2}$$

These harmonics from the shaft speed oscillations are present in the stator current, complicating the estimation of the PSHs.

Equation (1) can be used for speed estimation [2, 3, 26–28]. A sample current spectrum of a motor with its slot harmonics is shown in Fig. 1 for different values of ν. The motor used was a three-phase machine with $R = 48$ rotor slots and $p = 3$ pole pairs loaded by a dynomometer to run at $s = 0.0171$ or 1180 rpm. Typically, the slot harmonics with $k = 1$ and with $n_d = 0$ are the most pronounced in the current spectrum [2, 29]. For a given n_d, the slot harmonics differ exactly by $2f$ in (1). Of course, harmonics that are distinct from integer multiples of the utility line frequency will only appear, for an induction motor, when the machine is under some non-zero mechanical load. Generally, pumps, fans and other industrial and commercial motors will be operated with some load that creates a non-zero slip. Variations in slip can occur under normal operation if the mechanical load varies. As described in the references below, variations in slip may also indicate pathological conditions occurring or developing in the machine.

Analogue techniques [28, 30] have been implemented to track these harmonics. The performance of these approaches can be limited in terms of accuracy, linearity, resolution, speed range or speed of response [31]. Any analogue filtering can require extremely complex circuitry and any output signal can be corrupted by noise. Digital techniques employing the discrete Fourier transform (DFT) and its computationally efficient fast Fourier transform implementation were developed [27] to overcome the flaws in the analogue methods. These DFT methods were limited by the uncertainty principle, that is, the trade-off between high frequency resolution and the response time to changes of speed that deteriorates with long data records. Parametric estimation [2, 3, 26] of the current spectrum has been used to overcome the limitations of the DFT by attempting to model the process that generates the data using a priori knowledge. However, these approaches use digital filters that add computation time and noise sensitivity. Longer computations times can reduce any advantage these parametric methods may have over methods employing the DFT.

Some research has been done to combine the DFT methods and parametric estimation methods [2, 3]. In [2], the techniques do a successful job in tracking the slot harmonics in estimating speeds in a controlled environment, that is, monitoring a single motor. The authors make use of the periodicity of the slot harmonics by aliasing the spectrum such that these harmonics line up to increase detectability. We observe that the PSH is the most pronounced slot harmonic in the motors used in our experiments. The methods in this paper, therefore, focus on the PSH as the strongest signal source for the speed estimator.

There are certain trade-offs and data acquisition considerations that must be made when deciding on the proper methods for detecting these speed-dependent rotor slot harmonics, outlined in the following sections.

3 Data acquisition

On the electric utility, an energy meter or monitor will measure a load current with a large line frequency, for example, 60 Hz, component that typically dominates the current signal. To improve

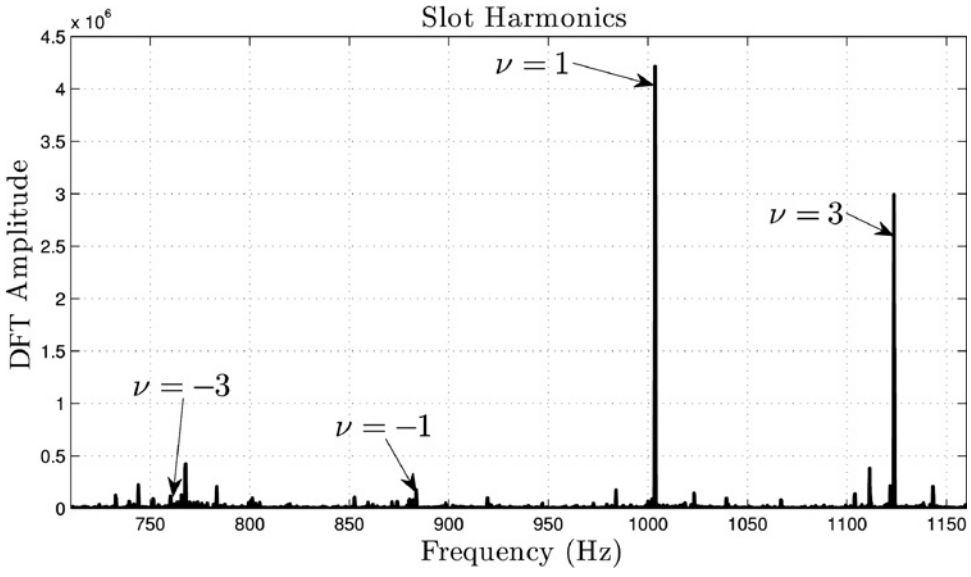

Fig. 1 *Slot harmonics for a motor at rated mechanical load with the following parameters: $f = 60$, $k = 1$, $R = 48$, $n_d = 0$, $s = 0.0171$ or 1180 rpm*

Harmonics shown in the figure are labelled with the corresponding value of ν

the detectability of lower amplitude, high-frequency slot harmonics, a utility frequency notch filter can eliminate the large line frequency component before the data acquisition hardware in the NILM samples the current. In Fig. 2, the stator current signal is processed by a 60 Hz notch filter. The core of the notch filter consists of a cascade of two second-order band-stop filter stages constructed using the UAF42 from Texas Instruments. Each second-order stage is configured with a Q of 11/3, although the value is adjustable in the field with our hardware. The centre frequency is placed on the utility line frequency, nominally 60 Hz in our experiments. Relatively low Q, as in our experiments, for each stage means that utility fundamental frequency content is well-attenuated even for small variations in utility frequency. In practice, the filter is configured to provide good dynamic range, that is, a reasonable bit-resolution, for the slot harmonics of interest. This varies with the amplitude of the slot harmonics under observation. However, our field experience indicates that the configuration shown in Fig. 2 works well for a wide range of induction machines. The output of the band-stop filters is amplified by a gain stage and later filtered by a passive antialiasing filter. The output buffer drives the input of the NILM data acquisition hardware. The notch filter stage allows for improved signal detectability of the smaller slot harmonics. By removing the large dominant line frequency, the smaller harmonic signals can then be amplified, increasing the overall signal-to-noise ratio by reducing the effect of quantisation noise in the analogue-to-digital converter of the NILM.

With the line frequency current content eliminated, a monitoring system can focus gain and sampling resolution on the higher frequency, smaller slot harmonics. The frequency band for these harmonics depends on motor slip, complicating the search for the PSH in order to determine rotor speed. A few observations about practical induction motors quickly narrow the search for slot harmonics and speed information.

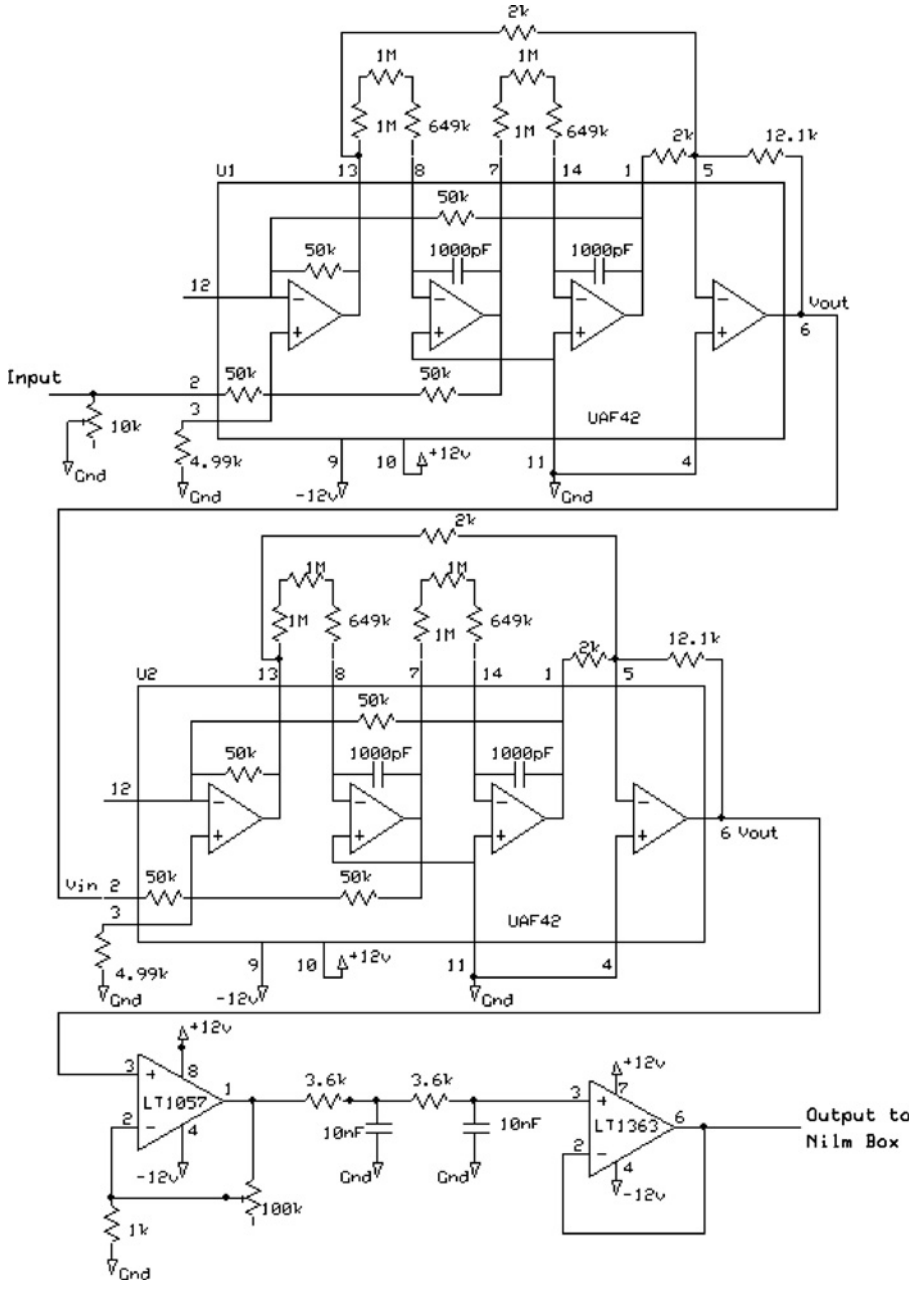

Fig. 2 *Schematic of the 60 Hz notch filter circuit*

Circuit notches the 60 Hz frequency, amplifies the signal and sends the signal through an antialiasing filter

IET Electr. Power Appl., 2015, Vol. 9, Iss. 5, pp. 388–396

Table 1 Maximum slip for speed estimation in a 120 Hz harmonic band

	p			
R	1	2	3	4
16	0.1247	0.2494	0.3742	0.4989
20	0.0997	0.2000	0.3000	0.4000
24	0.0833	0.1667	0.2492	0.3333
28	0.0714	0.1428	0.2142	0.2856
32	0.0622	0.1244	0.1875	0.2489
34	0.0586	0.1172	0.1758	0.2344
40	0.0500	0.1000	0.1500	0.1989
44	0.0453	0.0906	0.1358	0.1811
48	0.0417	0.0833	0.1250	0.1667
52	0.0383	0.0767	0.1150	0.1533
56	0.0356	0.0711	0.1067	0.1422
60	0.0333	0.0667	0.1000	0.1333

4 Limitations on slip

For high-efficiency induction motors, the slip s usually does not exceed 5% and possibly less. This assumption leads to interesting simplifications when searching for the PSH. The PSH refers to the slot harmonic with $\nu = 1$, $k = 1$ and $n_d = 0$ in (1) and is used in speed estimation algorithms since it is often the most pronounced [2, 29]. The slot harmonics for different values of ν differ by $2f =$ 120 Hz. If the PSH was confined to a 120 Hz window under these practical limitations of slip, there would be no ambiguity in determining the window of the PSH.

To illustrate the potential utility of the proposed approach, Table 1 tabulates the maximum slip for different values of R and p for which the PSH would be confined to a 120 Hz window. This table is populated by determining the value of slip, increasing from zero slip that results in an integer increase in the bracketed argument of (1). For example, for a motor with $R = 60$ and $p = 1$, a maximum slip of $s = 0.033$ would need to be assumed in order to constrain the PSH to a 120 Hz wide window. This assumption might be unreasonable because it would be possible for the motor to be running with a slip of 0.04. In this situation, there would be some ambiguity in determining in which window the PSH lies. On the other hand, a motor with $R = 48$ and $p = 3$ can have a maximum slip of $s = 0.125$ to unambiguously determine the window of the PSH. This slip satisfies any reasonable low-slip assumptions. Most motor designs (rotor bar count and pole pair choices) result in motors that exhibit PSHs in an unambiguous 120 Hz band over normal slip operating ranges.

5 Speed estimation with slot harmonics

With a 'low-slip' assumption in which the PSH is restricted to a single 120 Hz wide frequency window, an algorithm can be developed for using slot harmonics to determine motor operating speed just after startup in a multi-load/multi-motor environment. To demonstrate the effectiveness of the algorithm, the speed estimation method was conducted with the following two motors. The first motor (Motor 1) was a three-phase motor from an HVAC evaporator in an air-handling unit. Motor 1 has $R = 48$ rotor slots and $p = 3$ pole pairs. The second motor (Motor 2) is a single-phase, capacitor-start, line-to-line machine from a fresh-air ventilation unit with $R = 34$ rotor slots and $p = 1$ pole pairs. Note that the presence of a starting device, for example, the capacitor starter, or a soft starter, or a frequency converter, will not generally create a problem for the proposed method. The NILM uses transient information as a 'trigger' to make a comparison between pre-trigger and post-trigger, steady harmonic content changes. Starting devices do not eliminate a startup transient, they merely change the fingerprint or signature that the NILM must apply as a trigger. As long as critical slot harmonics remain observable in steady-state operation, the startup transient can be used to created 'before-and-after' windows for further examination with the harmonic estimation strategy described below.

Fig. 3 shows an experiment in which the first motor is activated, continues to run in steady-state operation, and then the second motor activates. The NILM identifies transients with spectral envelopes that are amplitude normalised for easy comparison against transient fingerprints [32]. The unit normalisation in Fig. 3 corresponds to an observed peak current of 26 A. Region A marks the start of Motor 1 (the evaporator motor). Region B marks the turn-on transient of Motor 2. A spectral envelope of the current that correspond to 'real' power as calculated by the NILM are shown in Fig. 4.

These two motors meet the 'low-slip' conditions summarised in Table 1. A non-intrusive monitor can therefore expect that the PSH for Motor 1 will be between 900 and 1020 Hz, whereas the PSH for Motor 2 will be between 1980 and 2100 Hz. The location of the PSH for a given slip, or the operating slip given an observed PSH, can be determined using (1).

As Motor 1 turns on, the NILM characterises this new load from its transient turn-on response and spectral envelope, as shown in Fig. 4. The steady operating speed of Motor 1 can be determined by comparing the frequency content of the aggregate current prior to the activation of Motor 1 to the frequency content in a current window just after the motor enters steady operation. That is, the NILM saves a 'pre-transient' and 'post-transient' window of current data when a motor starts. These two windows can be analysed for differences in frequency content to find the location of the newly introduced PSH and therefore to determine motor speeds.

The frequency window of interest to locate the PSH for Motor 1 is shown in Fig. 5. Using 5 s of current data, sampled at 7800 Hz, the location of the PSH can be estimated to be about 994 Hz by finding the location of the maximum value within the window. Using (1), the speed can be estimated to be about 1167 rpm. Not that, by simply

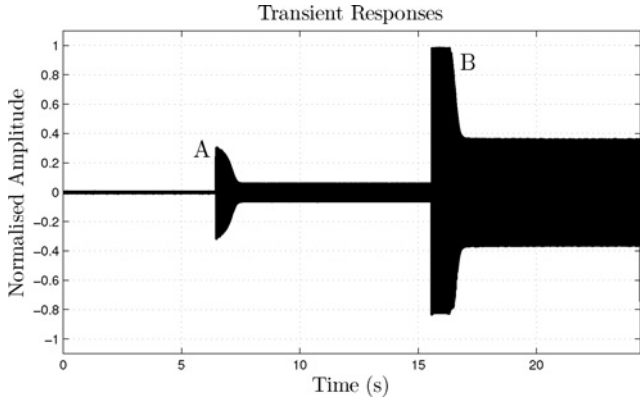

Fig. 3 *Amplitude of measured phase current with transient responses for Motors 1 and 2*

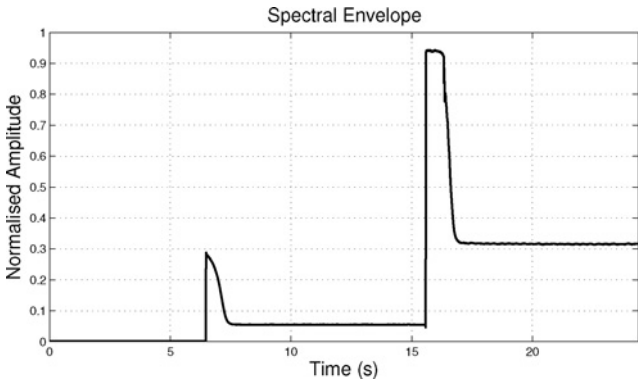

Fig. 4 *Spectral envelope corresponding to real power in steady-state operation*

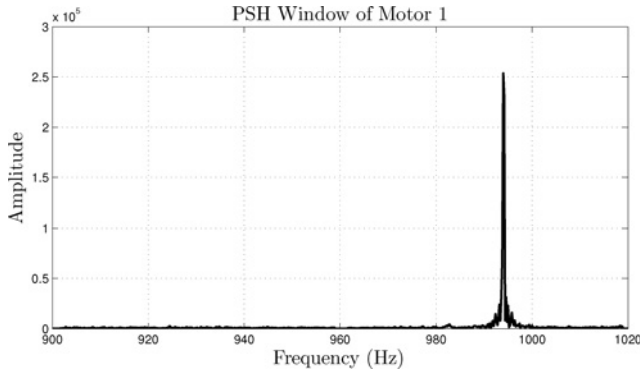

Fig. 5 *Partial current spectrum with Motor 1 running*

taking the maximum value within the PSH frequency window, the resolution of the frequency and associated speed estimate is limited to the size of the DFT frequency bins, which is determined by the total duration of sampling. With easy and verifiable assumptions, the estimate of the PSH and the motor's speed can be improved.

The energy of the PSH in the DFT is actually spread over several frequency bins implying that there is insufficient resolution to determine the PSH precisely. One way to obtain finer resolution would be to sample data over a longer interval, decreasing the frequency bin size. This is unattractive for motor monitoring, as the speed of the motor is more likely to vary during a longer interval, smearing the PSH localisation process. A second approach relies on the easily verified assumption that only one motor was activated in the 'pre-transient' and 'post-transient' current windows for evaluating the PSH. In this case, the coarse DFT bins can be examined to more closely localise the exact frequency of the newly appearing PSH frequency content.

Consider the illustrative example in Fig. 6 of the DFT of a pure sinusoid wave with a frequency of 994.34 Hz. In Fig. 6*a*, the DFT of 5 s of this pure sine wave is shown. Compare this result with that of Figs. 6*b* and *c* in which the data length is reduced to 0.5 and 0.05 s, respectively. The energy of the signal is spread over an increasingly wider frequency band as the sampling window duration decreases. However, shorter windows are attractive because the motor is more likely at a quasi-static operating speed during the brief window interval.

When dealing with the short, 0.05 s long data, each bin of the resulting DFT is 20 Hz wide. Frequency estimates for the PSH are nominally limited by this DFT resolution. The situation can be improved by taking advantage of the fact that if only one sine wave has appeared in the window, there is a unique mapping between any new sine wave amplitude and frequency and the associated frequency bin content. An optimisation routine can pick the frequency and amplitude of a sinusoid whose DFT is the best fit (in the minimum squared error sense) for the observed data over the entire frequency neighbourhood around the peak.

Mathematically, this involves a search over the candidate frequency and amplitude. Let $O(k)$ be the current DFT spectrum of the observed data with frequency index k, as shown in Fig. 6*c*. Let $S(k)$ be the DFT of the underlying sine wave $s(t) = \sin(2\pi ft)$ with frequency f. The routine searches to find a frequency f that minimises the error

$$E(f) = \sum_k \left| C_f \cdot S(k) - O(k) \right|^2 \tag{3}$$

with the normalising scale factor

$$C_f = \sqrt{\frac{\sum_k O^2(k)}{\sum_k S^2(k)}} \tag{4}$$

The frequency (and scale factor) that produces the least amount of error is the output of the routine. For the 0.05 s window in Fig. 6*c*, the estimator selects exactly 994.34 Hz as there is no noise to corrupt the data. By assuming the addition of only a single new sine wave in the 'post-trigger' or 'post-transient' window, the algorithm can determine the frequency of this new sine wave with a resolution that is finer than the quantised bin resolution of the DFT.

This idea can be applied to the actual data taken from Motor 1 shown in Fig. 5. Using a 5 s window of data sampled at 7800 Hz, the estimate of the PSH for Motor 1 is 993 Hz. A speed estimate of 1166.250 rpm is then calculated from this estimate of the PSH.

The results of applying the routine to shorter lengths of data are shown in Fig. 7. The frequency content for 0.5 s of data of Motor 1 near the PSH is shown by the solid line in Fig. 7*a*. The routine

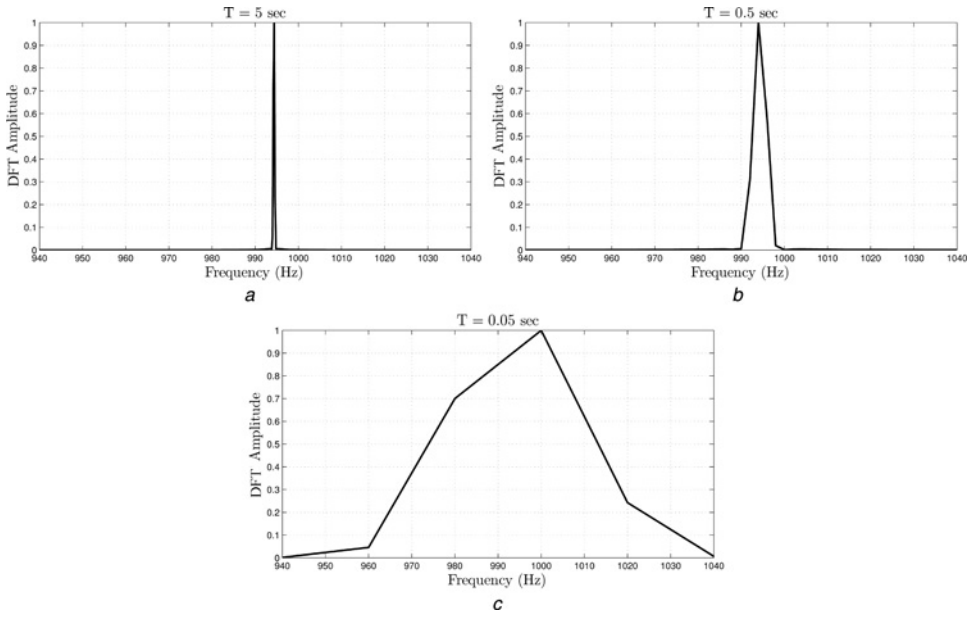

Fig. 6 *DFT of a pure sinusoid wave with a frequency of 994.34 Hz*

a DFT is shown for the sinusoid with a sampling time of 5 s

b, c Energy in the peak spreads out over several frequency bins as the sampling duration decreases

IET Electr. Power Appl., 2015, Vol. 9, Iss. 5, pp. 388–396

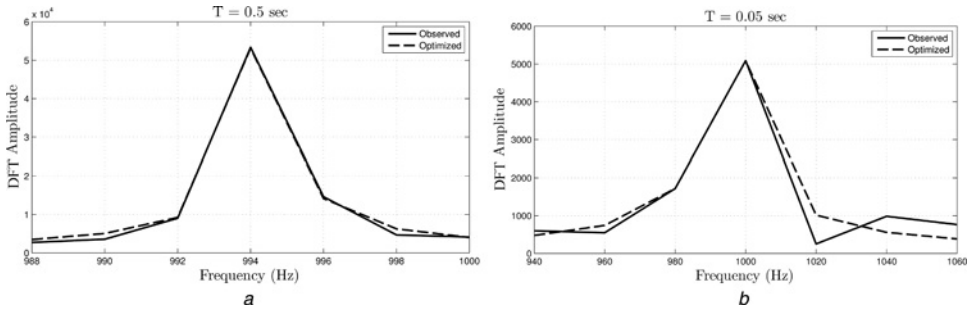

Fig. 7 *Observed PSH and DFT of the best-fit sine waves*

a Observed PSH is shown in the solid line. The dotted line is the DFT of the best-fit sinusoid. The sampling time is 5 s
b Observed PSH is shown in the solid line. The dotted line is the DFT of the best-fit sinusoid. The sampling time is 0.5 s.

finds the frequency of a sinusoid whose DFT best matches with the observed data, in this case 992.7 Hz. Again, the routine is making the assumption that there is only a single, pure sinusoid responsible for all observed frequency content. The dotted line in Fig. 7*a* is the DFT of a 0.5 s sinusoid with a frequency of 992.7 Hz. The DFT of this sinusoid closely matches with that of the observed data (solid line) in the region of interest. A speed estimate of 1165.870 rpm is then calculated from the estimate of the PSH. This is repeated for 0.05 s of data in Fig. 7*b*. The estimated PSH is 992.08 Hz and the corresponding speed estimate is 1165.100 rpm.

This estimation routine maintains accurate speed estimates even while using shorter duration windows of data. Table 2 displays the results of the estimator for different sampling times. These results show how a remarkably short duration windows of motor current can be used by a non-intrusive monitor to quickly estimate the speed of a motor after turn-on, a very useful estimate for diagnostics and fault detection.

The speed estimation algorithm can run continuously as new loads turn on and off. There are scenarios that may complicate speed tracking. If two motors with identical parameters are operating, the worst case scenario would have both motors running at the same speed. In such a case, the PSH of each motor would be at the exact same location. To prevent this, if possible, motors can be selected in a plant so that such a scenario could not occur. In this experiment, the parameters of the motors differentiated the machines, resulting in the PSH of each motor appearing in separate windows. Selecting motors for their ability to be tracked non-intrusively may be an option in 'ground-up' designs of a plant involving several motors.

Table 2 Optimisation routine PSH and speed estimates at different sampling times

T, sec	Line cycles	PSH, Hz	Speed, rpm
5	300	993.080	1166.350
3	180	992.929	1166.161
1	60	992.760	1165.950
0.5	30	992.700	1165.870
0.1	6	992.960	1166.200
0.05	3	992.080	1165.100
0.0333	2	997.200	1171.500
0.0166	1	990.140	1162.675

Also complicating speed estimation, the utility line has its own set of harmonics which are visible in the current spectrum. The 17th harmonic at 1020 Hz could be troublesome in trying to identify the PSH of Motor 1 in this example. Fortunately, as these potentially interfering harmonics are located at integer multiples of 60 Hz, we can easily filter them out using the digital filter $y[n] = x[n] - x[n-N]$ where N is the number of sample points per 60 Hz line cycle (in this paper, all data are sampled at 7.8 kHz, which corresponds to $N = 130$). This filter will notch out all the integer multiples of the line frequency before data is passed to the algorithm for speed estimation.

Motor 2's eccentricity harmonics represent a potential second complication in this experiment [16]. Motor 2 is loaded with a fan which exacerbates eccentricities. Fig. 8*a* shows the window of interest for the PSH of Motor 1 when both motors are running. Here, the motors produced slot harmonics that are larger in amplitude than any of the eccentricity harmonics. This is likely to be a typical situation in a relatively healthy motor. That is, the development of shaft eccentricity can be tracked and trended over time, typically assuming that the PSH is a larger signal than the eccentricity harmonics in an initially health machine. As eccentricities develop, the PSH speed estimator can actually be used to track the extent of eccentricity as a diagnostic and prognostic indicator.

Specifically, tracking eccentricity harmonics may be possible by first estimating the speed of an eccentric motor. Once the slip is estimated, all possible eccentricity harmonics can be tabulated and tracked. Changes in the observed amplitudes of these eccentricity harmonics can be used to diagnose the health of the motor. Moreover, the above algorithm can use the knowledge of eccentricity harmonics to make better speed predictions by

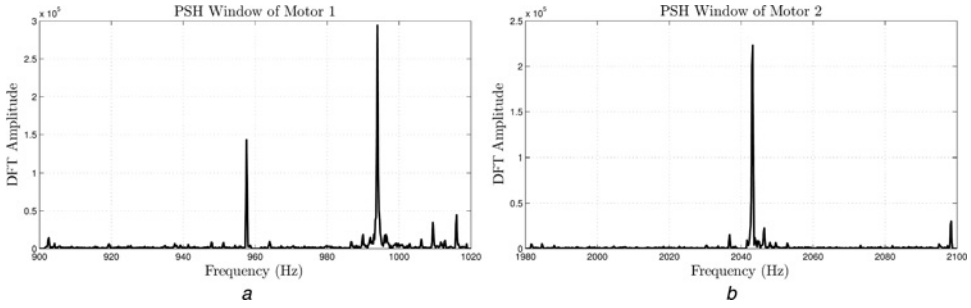

Fig. 8 *Aggregate current spectrum with both motors running*

a Current spectrum in the PSH window of Motor 1
b Spectrum in the PSH window of Motor 2

properly including the effects of the eccentricity harmonics in the observed frequency content. The PSH for Motor 2 was determined to be between 1980 and 2100 Hz. The current spectrum at these frequencies is shown in Fig. 8*b*. The PSH for Motor 2 is estimated at 2046.28 Hz which corresponds to 3505.20 rpm.

In the next two sections, we demonstrate applications of this non-intrusive speed estimation algorithm for motors in machine plants associated with HVAC. A typical HVAC plant in a residence or medium-sized commercial building consists of three motors: two for the evaporator and compressor fans, and one for a refrigerant compressor. A reciprocating compressor is a positive displacement design used to compress and pump refrigerants and other gases. In larger installations, a three-phase induction motor drives the crank shaft of the reciprocating compressor, which causes motion of the pistons. Knowledge of the compressor motor speed and the induction fan motor speeds in an HVAC plant are essential pieces of information for performing non-intrusive electrical diagnostics on these systems [33].

6 Reciprocating compressor diagnostics

HVAC plants are notorious energy wasters. Because they operate under closed-loop feedback control, they will maintain occupant comfort, for example, they will show no visible signs of a pathological condition until the condition becomes crippling to the plant. As an HVAC plant gradually develops an increasingly severe fault, it will consume more and more energy over time trying to maintain a setpoint. A speed estimate of the compressor operation can be used to identify pathological operation [33].

Non-intrusive electrical fault detection works to recognise faulted conditions for specific equipment in an aggregate current signal, conditions that reliably correspond to mechanical faults in the system. For example, when the NILM can disaggregate or observe compressor voltage and current signals, these waveforms can be used to 'invert' the induction motor model equations to calculate the torque and speed of the motor [33]. The motor shaft speed, along with the driving torque, can be used to calculate the load torque on the crankshaft. The crankshaft load torque signal is sensitive to valve and other mechanical faults in the compressor. That is, with knowledge of compressor shaft speed, it is possible to use a NILM as a platform for identifying mechanical faults like valve failures in the compressor.

To develop these fault detection techniques in [33], a custom shaft extension was installed on the integrated induction machine moving a compressor. An encoder with 2500 counts is mounted on the extension to provide speed readings. This intrusive modification of the reciprocating compressor was used as instrumentation to demonstrate the potential of our non-intrusive speed estimation based on PSHs.

The non-intrusive speed estimation algorithm presented in the previous section is capable of providing a speed estimate for diagnostic routines with no mechanically invasive procedures. The instrumented compressor with induction motor was operated with a pressure difference of 70 psi. To evaluate the effectiveness of the non-intrusive speed estimator, the shaft encoder data was processed with a running average of 1 s with a 50% window overlap to compute speed. The encoder speed measurement is shown as the solid line in Fig. 9. The non-intrusive speed estimate using the same data window length and 50% overlap is shown as the dotted line in Fig. 9. The very slight speed change that occurs around 50 s in Fig. 9 resulted from a disturbance in the local utility frequency at that point during the experiment. Both the high-resolution encoder and the speed estimator tracked the rotor speed through this disturbance.

Fig. 9 illustrates that the estimator accurately tracks the motor speed in comparison to a high resolution tachometer. The essential difference is that the non-intrusive speed estimation algorithm did not require any physical modification of the compressor.

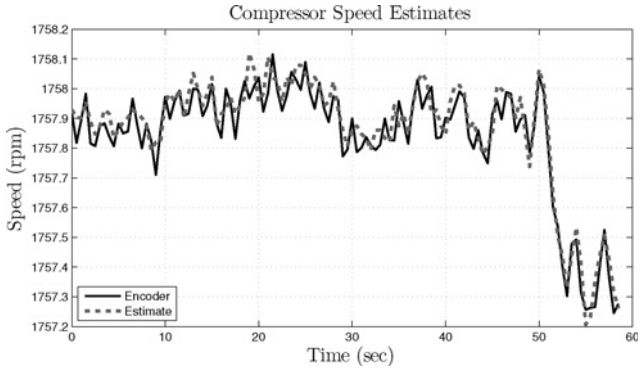

Fig. 9 *Speed estimate comparison of a compressor with a steady tank at 70 psi*

Solid line is the estimate from the custom mounted encoder and the dotted line is the non-intrusive speed estimate

7 Ventilation fan

Motor 2, described previously, is a fresh air ventilation fan. This fan was installed at a local school building to test the ability to determine motor speed by locating the PSH associated with the machine. This test is a 'real world' experiment where a NILM was used to find and identify the PSH from an aggregate current stream with other loads operating in the building.

The NILM installed at this school test site includes the notch circuitry shown in Fig. 2. It was installed at the service entry to the main panel in the school machine room, a panel that served both heating equipment and also an information-technology computing room in the school. This particular testing reveals how the NILM can detect and determine motor operating speed in an operating background with other loads active. The raw current drawn by the panel was observed and processed by the NILM, including the pre-transient current, and also the transient response of the motor as it was activated.

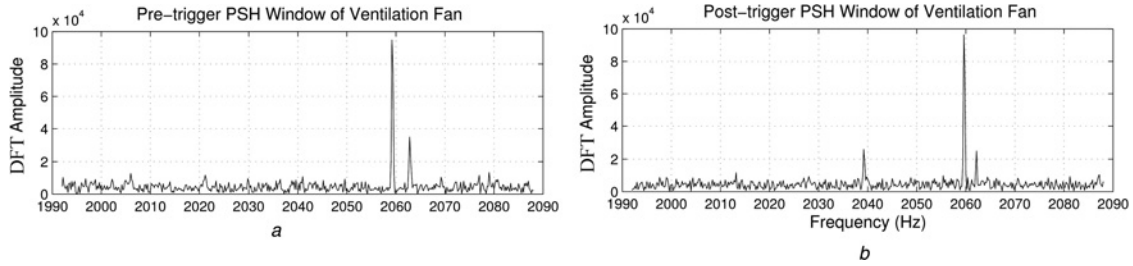

Fig. 10 *DFT of the current before turn-on and after the motor has reached steady state*

a Pre-trigger PSH window of ventilation fan
b Post-trigger PSH window of ventilation fan

IET Electr. Power Appl., 2015, Vol. 9, Iss. 5, pp. 388–396

Table 3 PSH estimation for various lengths of times

Time length	PSH	rpm
5	2037.651	3489.972
1	2039.689	3493.568
5	2039.237	3492.771
10	2039.239	3492.774

The PSH of the ventilation fan can be found by comparing the DFT window of the motor current before and after the motor has turned on. Fig. 10*a* shows the DFT of the current during the pre-trigger window before the motor has turned on. Fig. 10*b* shows the DFT of the current during the post-trigger window after the motor has turned on and reached steady state. These two time windows can be determined by the NILM, which recognise transients and can save windows of data before and after electrical events in the aggregate current data.

The PSH of the motor is visible in the post-trigger window near 2040 Hz. This 'new' frequency content is found by a threshold algorithm and comparison to the pre-trigger window. The estimation routine is then conducted to estimate the precise location of the harmonic. The results are tabulated in Table 3 for various window lengths.

8 Conclusions

It is often reasonable to assume that basic information about an electro-mechanical plant will be available for residential and industrial applications. For example, the torque-speed curve of an air handling motor or pump is often known, or could be obtained by or from a manufacturer. Similar information, for example, a fan curve relating shaft power and speed to air flow, can be found for common fans and, similarly, for pump heads. The experimental results presented here demonstrate how a NILM can determine electrical power [i.e. from spectral envelopes as shown in Fig. 4 and mechanical shaft speed (as shown in Table 2)] from a reasonably chosen aggregate power measurement where other loads may also be operating. In situations where data like torque-speed curves are known a priori, a NILM could use this information along with its measurements of electrical power consumption and motor operating speed to perform fault detection and diagnostics on critical energy consumers like air-conditioning and air-handling systems.

This paper illustrates how the known behaviour of motor harmonics could be exploited with reasonable assumptions about operating conditions to estimate speed in a non-intrusive setting. Spectral envelope computations are used to characterise the operating schedule of loads as they turn on. Once recognised as 'on', the current before and after the transient can be analysed to estimate the speed of the new motor joining the collection of operating loads on the monitored service. A fine estimate of speed can be calculated by employing an optimisation routine to find the frequency of a sinusoid that best matches with the spectral content of the observed data. This routine allows for smaller sampling windows to obtain desirable frequency resolution. This technique can be extended to estimate the speeds of multiple motors from one aggregate current signal.

Any load that exhibits a unique current harmonic that is not an integer multiple of the line frequency could be tracked using the method developed in this paper. Of course, the physical meaning of the tracked harmonic would vary with the load. For example, a converter-fed drive might 'hide' harmonics of the motor itself by filtering the harmonics before injection to the utility. On the other hand, depending on the drive construction, other useful information may appear on the utility side of the drive. Moreover, we have found that converter-fed motors generally retain their slot harmonic signatures when monitored on the 'motor-side' of the drive [32].

Of course, an unfortunate collection of loads could hinder the NILM's ability to detect operating speeds. In critical situations where non-intrusive monitor is desirable, motors might be selected during the design of a plant to enhance detectability.

9 Acknowledgments

This work was supported in part by The Grainger Foundation, the ONR Structural Acoustic program and the BP-MIT Research Alliance.

10 References

1 U.S. Department of Energy: 'The smart grid: an introduction' (World Wide Web Electronic Publication), 2008. Available at http://energy.gov/sites/prod/files/oeprod/DocumentsandMedia/DOE_SG_Book_Single_Pages.pdf
2 Hurst, K.D., Habetler, T.G.: 'Sensorless speed measurement using current harmonic spectral estimation in induction machine drives', *IEEE Trans. Power Electron.*, 1996, **11**, (1), pp. 66–73
3 Hurst, K.D., Habetler, T.G.: 'A comparison of spectrum estimation techniques for sensorless speed detection in induction machines', *IEEE Trans. Ind. Appl.*, 1997, **33**, (4), pp. 898–905
4 Thomson, W.T., Fenger, M.: 'Current signature analysis to detect induction motor faults', *IEEE Ind. Appl. Mag.*, 2001, **7**, (4), pp. 26–34
5 Thomson, W.T., Leonard, R.A., Milne, A.J., Penman, J.: 'Failure identification of offshore induction motor systems using on-condition monitoring', *Reliab. Eng.*, 1984, **9**, (1), pp. 49–64
6 Schoen, R.R., Habetler, T.G., Kamran, F., Bartfield, R.G.: 'Motor bearing damage detection using stator current monitoring', *IEEE Trans. Ind. Appl.*, 1995, **31**, (6), pp. 1274–1279
7 Guldemir, H.: 'Detection of airgap eccentricity using line current spectrum of induction motors', *Electr. Power Syst. Res.*, 2003, **64**, (2), pp. 109–117
8 Orji, U.A., Remscrim, Z., Laughman, C., *et al.*: 'Fault detection and diagnostics for non-intrusive monitoring using motor harmonics'. Twenty-Fifth Annual IEEE Applied Power Electronics Conf. and Exposition (APEC), 2010, Palm Springs, CA, February 2010, pp. 1547–1554
9 Cowan, A.: 'Review of recent commercial rooftop unit field studies in the Pacific Northwest and California'. Technical Report, New Buildings Institute, White Salmon, WA, 8 October 2004
10 Mowris, R.J., Blankenship, A., Jones, E.: 'Field measurements of air conditioners with and without TXVs', 2004
11 Hales, D., Gordon, A., Lubliner, M.: 'Duct leakage in new Washington state residences: findings and conclusions', *ASHRAE Trans. – Am. Soc. Heat. Refrig. Airconditioning Eng.*, 2003, **109**, (2), pp. 393–402
12 Srinivasan, K.: 'Measurement of air leakage in air-handling units and air conditioning ducts', *Energy Build.*, 2005, **37**, (3), pp. 273–277
13 Alger, P.L.: 'Induction machines, their behavior and uses' (Gordon & Breach Science Publishers, 1970)
14 Paris, J., Donnal, J., Leeb, S.: 'NilmDB: the non-intrusive load monitor database', *IEEE Trans. Smart Grid*, 2014, **5**, (5), pp. 2459–2467
15 Nandi, S., Ahmed, S., Toliyat, H.A.: 'Detection of rotor slot and other eccentricity related harmonics in a three phase induction motor with different rotor cages', *IEEE Trans. Energy Convers.*, 2001, **16**, (3), pp. 253–260
16 Benbouzid, M.E.H.: 'A review of induction motors signature analysis as a medium for faults detection', *IEEE Trans. Ind. Electron.*, 2000, **47**, (5), pp. 984–993
17 Kliman, G.B., Koegl, R.A., Stein, J., Endicott, R.D., Madden, M.W.: 'Noninvasive detection of broken rotor bars in operating induction motors', *IEEE Trans. Energy Convers.*, 1988, **3**, (4), pp. 873–879
18 Kliman, G.B., Stein, J.: 'Methods of motor current signature analysis', *Electr. Mach. Power Syst.*, 1992, **20**, (5), pp. 463–474
19 Hargis, C., Gaydon, B.G., Kamash, K.: 'The detection of rotor defects in induction motors'. Proc. IEE EMDA Conf., London, 1982, pp. 216–220
20 Nandi, S., Toliyat, H.A., Li, X.: 'Condition monitoring and fault diagnosis of electrical motors – a review', *IEEE Trans. Energy Convers.*, 2005, **20**, (4), pp. 719–729
21 Elkasabgy, N.M., Eastham, A.R., Dawson, G.E.: 'Detection of broken bars in the cage rotor on an induction machine', *IEEE Trans. Ind. Appl.*, 1992, **28**, (1), Part 1, pp. 165–171
22 Schoen, R.R., Habetler, T.G.: 'Effects of time-varying loads on rotor fault detection in induction machines', *IEEE Trans. Ind. Appl.*, 1995, **31**, (4), pp. 900–906
23 Schoen, R.R., Lin, B.K., Habetler, T.G., Schlag, J.H., Farag, S.: 'An unsupervised, on-line system for induction motor fault detection using stator current monitoring'. Conf. Record of the 1994 IEEE Industry Applications Society Annual Meeting, 1994, 1994, pp. 103–109
24 Benbouzid, M.E.H., Vieira, M., Theys, C.: 'Induction motors' faults detection and localization using stator current advanced signal processing techniques', *IEEE Trans. Power Electron.*, 1999, **14**, (1), pp. 14–22
25 Cameron, J.R., Thomson, W.T., Dow, A.B.: 'Vibration and current monitoring for detecting airgap eccentricity in large induction motors', *IEE Proc. B [see also IEE Proc., Electr. Power Appl.] Electr. Power Appl.*, 1986, **133**, (3), pp. 155–163
26 Ferrah, A., Hogben-Laing, P.J., Bradley, K.J., Asher, G.M., Woolfson, M.S.: 'The effect of rotor design on sensorless speed estimation using rotor slot harmonics identified by adaptive digital filtering using the maximum likelihood approach'.

Thirty-Second IAS Annual Meeting, IAS'97, Conf. Record of the 1997 IEEE Industry Applications Conf., 1997, October 1997, vol. 1, pp. 128–135
27 Ferrah, A., Bradley, K.G., Asher, G.M.: 'Sensorless speed detection of inverter fed induction motors using rotor slot harmonics and fast Fourier transform'. IEEE Power Electronics Specialist Conf., 29 June–3 July 1992, vol. 1, pp. 279–286
28 Ishida, M., Iwata, K.: 'A new slip frequncy detector of an induction motor utilizing rotor slot harmonics', *IEEE Trans. Ind. Appl.*, 1984, pp. 575–582
29 Nandi, S.: 'Modeling of induction machines including stator and rotor slot effects'. Conf. Record of the 38th IAS Annual Meeting. Industry Applications Conf., 2003., 2003, vol. 2
30 Zinger, D.S., Profumo, F., Lipo, T., Novotny, D.W.: 'A direct field-oriented controller for induction motor drives using tapped stator windings', *IEEE Trans. Power Electron.*, 1990, **5**, (4), pp. 446–453
31 Ferrah, A., Bradley, K.J., Hogben-Laing, P.J., *et al.*: 'A speed identifier for induction motor drives using real-time adaptive digital filtering', *IEEE Trans. Ind. Appl.*, 1998, **34**, (1), pp. 156–162
32 Paris, J.: 'A comprehensive system for non-intrusive load monitoring and diagnostics'. PhD dissertation, Massachusetts Institute of Technology, Department of Electrical Engineering and Computer Science, September 2013
33 Schantz, C.J.: 'Non-intrusive fault detection in reciprocating compressors'. Master's thesis, Massachusetts Institute of Technology, Cambridge, MA, June 2011